13th Australasian Fluid Mechanics Conference
Monash University, Melbourne, Australia
13-18 December 1998

Measurements of Velocity and Vorticity in Grid Turbulence using PIV

D. Nicolaides, D. Honnery and J. Soria
Department of Mechanical Engineering,
Monash University, Clayton, Victoria

ABSTRACT

This paper presents the results of an experimental investigation of the turbulent flow behind a grid using cross-correlation Particle Imaging Velocimetry (PIV). Presented are measurements of the velocity and vorticity fields along with a statistical description of the flow.

INTRODUCTION

Previous measurements undertaken in grid generated turbulence are generally limited by their reliance on single point temporal data and, where possible its transformation using, for example, Taylors hypothesis to spatial data. The particle imaging velocimetry (PIV) technique allows direct measurement of the instantaneous spatial velocity field in a flow thus removing any uncertainty that may stem from such temporal transformations. From these spatial velocity fields, spatial velocity gradients and hence vorticity fields may be obtained. These field measurements also provide a spatial statistical description of the flow, which until recently was only obtainable from computational data.

In this paper we present cross-correlation PIV measurements of the spatial velocity and vorticity fields in the turbulent flow behind a grid located in a water tunnel. From these basic measurements statistical descriptions of velocity, velocity gradient and vorticity fields are presented.

EXPERIMENTS

Measurements of the turbulent field behind a grid where undertaken in the vertical closed-circuit water tunnel shown in figure 1. The working section has internal dimensions 250mm×250mm and 1400mm in length. Water is pumped into the settling chamber through a spray system. The settling chamber contains four turbulence damping screens and a single plastic honeycomb. Water is accelerated into the working section through a contraction with a 16:1 area ratio. The turbulence generating grid is mounted 30mm downstream of the contraction exit and is constructed from 6mm diameter stainless steel rod with a grid spacing of M=30mm.

The water in the tunnel is seeded with hollow glass spheres with mean diameter 11μm and S.G=1.1. Illumination of these glass spheres, or tracer particles, in the measurement plane is provided by two Spectra Physics 400mJ pulsed Nd:YAG lasers each having a firing frequency of 12Hz. The laser beams are aligned so as to be coincident upon the sheet forming optics which produce the imaging plane for the PIV measurement. The imaging plane is centrally located in the working section for all measurements and is approximately 1.5mm thick.

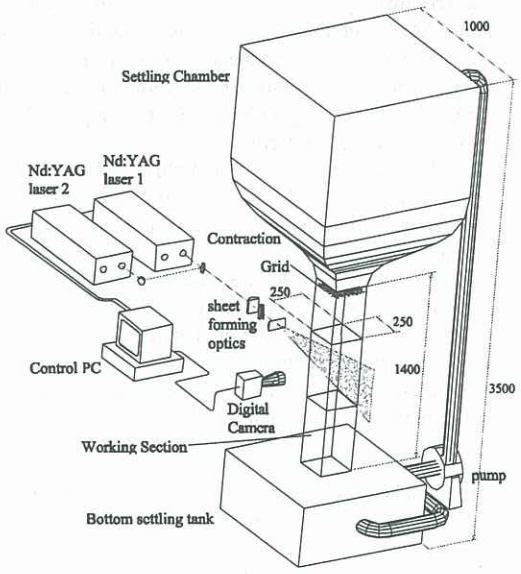

Figure 1: Water tunnel and experimental set-up.

Image acquisition was performed using a Kodak Megaplus XHF CCD camera (1000×1000 pixels) with an intensity resolution of 8 bit and maximum framing rate of 30Hz. A Data Translation IC-PCI digital frame grabber card was used to acquire images from the digital camera. The maximum framing rate, limited by the transfer time from frame grabber memory to the computer memory was 22Hz.

Calculation of the velocity field requires collection of two images. The time required between the images depends on the average speed of the water tunnel and is limited by the firing rate of the lasers and the time required to collect each image. To maximise the data collection for a variety of settings, a number of different image collection techniques had to be used. These involved; minimising the separation time between each single image to ensure minimum flow displacement between each image pair, varying the separation time between each image pair to maximise the total data collection, and when these were not possible, typically at high water speeds, using a double exposure technique to produce an image pair.

The digital cross-correlation PIV technique developed by Soria (1993) was used to obtain

velocity fields from the image pairs. This is an iterative technique which involves dividing each image into sub-image analysis regions, typically 32x32 pixels for single exposure image pairs and 64x64pixels for double exposed images, within which the local displacement vector is estimated. This is then used to offset the respective analysis region in the second image of the pair so that the dynamic range of the measurement is maximised (Soria (1996), Keane & Adrian (1992)). This becomes important when variations in a fluctuating turbulent flow exceed the dynamic range of the analysis region, as was the case in this study.

The number of vectors in each field depends on the image collection method. Typically single exposure image pairs resulted in approximately 2700 vectors per field, while double exposed images resulted in approximately 670. To reduce levels of random noise, the data acceptance levels were limited to 6 standard deviations, σ, from the mean. A spatial filtering routine, based on a second-order polynomial fit to the 12 nearest points using a Chi-square fitting procedure, was used to smooth the fields.

The number of vector fields collected for each experimental condition ranged from 60 to 100 depending on the collection technique required. For each condition, the average of the downstream, U, and cross-stream, V, velocities were determined and then subtracted from individual velocity fields to give the fluctuating velocity components, u and v, for each field. This allowed calculation of the root mean square velocities, u' and v' for each condition along with the root mean square turbulent velocity u,

$$u = \sqrt{(u'^2+v'^2)/2} \ .$$

Vorticity, ω_z, about the axis normal to the image plane is derived from the velocity field after calculation of the relevant velocity gradient fields. The velocity gradients at each point in the field are determined analytically from the second-order polynomial functions used to smooth the velocity.

Resolution of the collected images was typically 30μm/pixel. The error in the value of the mean down stream velocity, U, arising from uncertainty in determination of the location of the peak in the cross-correlation function for the sub-analysis regions plus any possible image pair time separation error is estimated to be ±1%. Error in the vorticity arises from two sources, random error in the velocity field and bias error from calculation of velocity gradients. Estimates of these errors in the present vorticity measurements from the experiments of Soria and Fouras (1995) result in uncertainties of about ±5-6%.

RESULTS AND DISCUSSION

Table 1 gives the conditions for the two data sets presented here for a turbulence grid with mesh spacing M=30mm. Data set A comprises measurements at a constant tunnel speed of 100mm/s at locations ranging from x/M of 20-33 downstream of the grid, while data set B is at a fixed downstream location, x/M=17, but at tunnel speeds varying from 125-200mm/s.

For the grid used in these experiments, the origin of the turbulent decay was found to occur at approximately x/M=10 placing both data sets in what is known as the initial period of turbulent decay (Batchelor, and Townsend, (1947, 1948)). In this region the turbulent field should exhibit a strong degree of isotropy and this is seen in the values of the turbulence intensities shown in Table 1. Values of u' and v', here normalised by the average downstream convective velocity, U, range from about 2-3.2% for data set A, and appear fairly constant for data set B at around 3.3-3.7%. The ratio of u'/v' lies between 1.04-1.2 which is typical for this type of experiment where some difference is expected in the individual components because of the direction of the convective velocity. Further evidence of the isotropy is seen in the almost constant mircoscale Reynolds number for data set A.

Table 1: Experimental Conditions for M=30mm Grid

	x/M	U mm/s	u'/U %	v'/U %	λ. mm	*Re $_\lambda$.
A1:	20	100	3.24	3.09	6.69	24
A2:	23	100	3.26	2.75	6.87	23
A3:	30	100	2.34	2.00	6.46	16
A4:	33	100	2.33	2.18	8.02	20
B1:	17	125	3.40	3.01	5.37	25
B2:	17	150	3.55	3.24	5.52	32
B3:	17	175	3.70	3.35	5.42	38
B4:	17	200	3.78	3.48	5.36	44

*Re $_\lambda$.=($u\lambda/\nu$)

The turbulent nature of the flow is illustrated by the results shown in figure 2 which presents a typical example of an instantaneous fluctuating velocity vector and voricity field for condition B4, Table 1. In this figure, the spatial coordinates are normalised by the measured Taylor microscale defined as,

$$\lambda = u^2 / \overline{\left(\frac{du}{dx}\right)^2} \ .$$

For the data shown in figure 2, λ=5.4mm and it can be seen that the captured field occupies around 4 Taylor microscales in each direction which is typical of most measurements. Structures in the flow are clearly evident and appear to be of the order of the Taylor scale.

Calculation of the vorticity may be checked by comparing the vorticity of a region of concentrated vorticity to its circulation,

$$\Gamma = \oint u_\theta dl = \int \omega \ dA \ .$$

Figure 3 shows a typical region for which both the area and line integrals may be determined. Agreement between circulation and the vorticity area integral typically yielded values of within 1-2%.

Probability distribution functions, pdf's, were calculated for both components of fluctuating velocity using all velocity vectors in the particular data set. Each pdf is normalised so that σ=1 and the area under the function is equal to one.

For data sets with smaller number of vectors the tails of the pdf's contain some noise which may be due to the lack of resolution in the outer percentiles. The pdf's of the fluctuating u component of velocity data set B is shown in figure 4. It is observed that for all data the distribution remains approximately Gaussian with a slight skewness towards negative values.

Similar comments may be made for the pdf of the v component

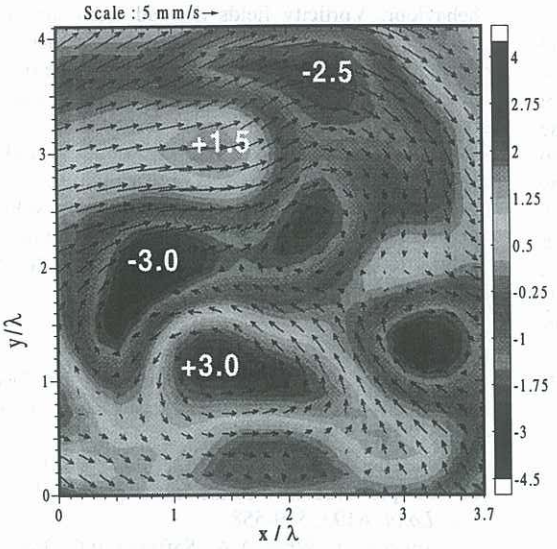

Figure 2: Instantaneous fluctuating velocity field shown by arrows, and vorticity field, normalised by the root mean square of the vorticity shown as contours, for condition B4, see Table 1.

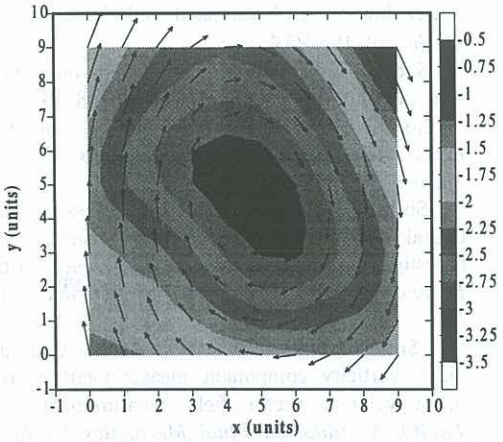

Figure 3: Typical region of concentrated voricity used to test calculation of vorticity from circulation. Center contour is –3.0, scale as for figure 2.

.Statistical moments were calculated from the pdf data. The third moment, S_3, skewness, and the fourth moment, S_4, kurtosis, were calculated for u and v. For these velocities of both data sets S_3 was found to almost equal to zero and S_4 equal to around 3, which are values associated with a Gaussian distribution. Previous experimental results by, for example, Townsend (1947, 1976) and Mohamed & LaRue (1990), showed similar values to these. Gaussian like behaviour in the velocity components may also be seen in the DNS data of Vincent & Meneguzzi (1991). It is worth noting that the trend for S_3 to increase with Reynolds number at a fixed downstream location seen by Mohamed & LaRue was not observed in the present data.

Probability distribution functions were calculated for vorticity, figure 5, and velocity gradients, figure 6. It was found that the transverse gradients, du/dy and dv/dx, had similar distributions and that the longitudinal gradients, du/dx and dv/dy, were also alike. From the data in these figures it is seen that the pdf's of vorticity and transverse gradients have a similar shape. Unlike the velocity components however, the vorticity and transverse gradient have a distribution that has non-Gaussian straight wings. The longitudinal gradients exhibit these wings, but mainly on the negative side of the distribution, and are skewed to the negative side

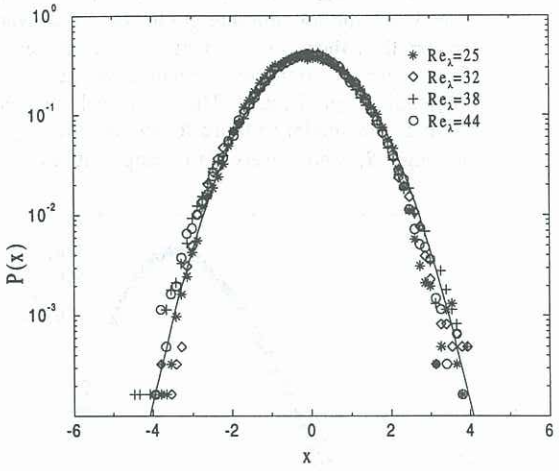

Figure 4: Probability density function of u velocity normalised by the standard deviation for data set B. Solid line is a Gaussian pdf distribution for comparison.

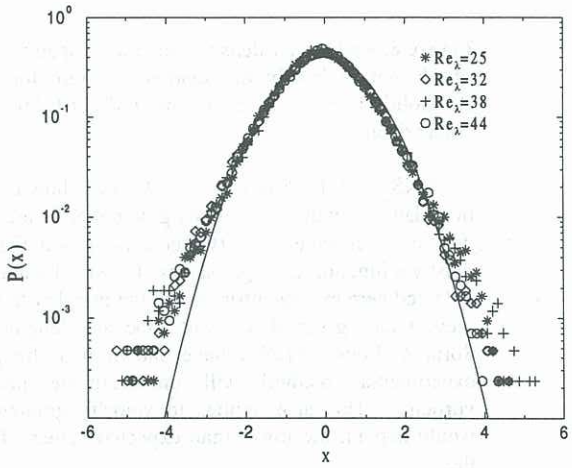

Figure 5: Probability density function of vorticity normalised by the standard deviation for data set B. Solid line is a Gaussian pdf distribution for comparison.

For the longitudinal gradients S_3 was typically between -0.1 to -0.3 while S_4 was typically 3.1-4.8. Townsend (1947) found values of S_3= -0.3 and S_4=3.3 from measurements of the longitudinal gradient du/dx in grid turbulence, while the DNS studies of Vincent & Meneguzzi (1991) and Jimenez *et al.* (1993) found S_3 to be around -0.5. The work by Jimenez *et al.* has shown

that S_4 increases from 4.2 for Re_λ=35, to 6.1 for Re_λ=168. Present measurements taken at a single location show an increasing trend in S_4 for the gradient *dv/dy* for Re_λ=25 to 44.

For the transverse gradients S_3 was typically zero and S_4 was typically between 3.7 and 4.2. DNS data for isotropic turbulence have shown S_3 to be zero. Jimenez *et al* (1993) observed more symmetry in the transverse gradients compared with the longitudinal. This is also observed in the present results. The results for S_4 by Jimenez *et al.* also show an increase in magnitude with Re_λ. The values they obtained, 5.7-9.4, were also larger than S_4 for the longitudinal gradients. These values are greater than those obtained here however trends show that S_4 for the transverse gradient is higher than for longitudinal gradient. The statistical moments for vorticity are similar to those for the transverse gradients although, S_4 is not observed to change with Re_λ.

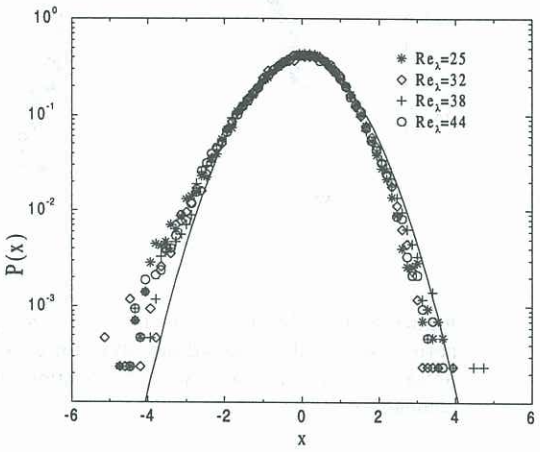

Figure 6: Probability density function of spatial gradient *(du/dx)* normailised by the standard deviation for data set B. Solid line is a Gaussian pdf distribution for comparison

DNS work by She *et al.* (1991) has shown that the non-Gaussian wings of velocity gradient pdf's are mainly due to small-scale velocity fluctuations and that S_3 is mostly a function of larger scales. The small values of S_4 obtained here may be attributed to the inability to resolve these scales given their short time and length scales. Soria & Fouras (1995) have shown that the present experimental method will underestimate peaks in vorticity. This also applies to velocity gradients and would explain the lower than expected values of S_4 for these.

CONCLUSIONS

The PIV measurements of the turbulent velocity field presented in this paper reveal a flow that closely approximates an isotropic turbulent field. Probability density functions of the turbulent velocity components appear to be approximately Gaussian in behaviour while spatial transverse and longitudinal velocity gradients demonstrate a degree of non-Gaussian behaviour. Vorticity fields derived from the spatial velocity gradients revealed regions of concentrated vorticity. The sizes of these regions are of the order of the Taylor microscale which for these experiments was found to be around 6mm. Probability density functions of the vorticity like the velocity gradients also show some non-Gaussian like behaviour.

The higher moments of the velocity, velocity gradient and vorticity fields show similar trends and values to previous experiments and also to data calculated from DNS.

REFERENCES

Batchelor, G.K., Townsend, A.A. (1947): Decay of vorticity in isotropic turbulence. *Proc. R. Soc. Lond.* A190, 534-550.

Batchelor, G.K., Townsend, A.A. (1948): Decay of isotropic turbulence in the initial period. *Proc. R. Soc. Lond.* A193, 539-558.

Jimenez, J., Wray, A.A., Saffman, P.G., Rogallo, R.S. (1993): The structure of intense vorticity in isotropic turbulence. *J. Fluid Mech.* 255, 65-90

Keane, R.D., Adrian, R.J. (1992): Theory of cross-correlation analysis of PIV images. *Scientific Research.* 49, 191-215.

Mohamed, M.S., LaRue, J.C. (1990): The decay power law in grid-generated turbulence. *J. Fluid Mech.* 219, 195-214.

She, Z. (1991): Intermittency and non-gaussian statistics in turbulence. *Fluid Dyn. Res.* 8, 143-158.

Soria, J. (1993): Particle image velocimetry. *Proc. International Colloquium on Jets, Wakes and Shear Layers, CSIRO*

Soria, J. (1996): An adaptive cross-correlation digital PIV technique for unsteady flow investigations. *First Australian Conference on Laser Diagnostics in Fluid Mechanics and Combustion.* 29-45.

Soria, J., Fouras, A. (1995): Accuracy of out-of-plane vorticity component measurement using in-plane velocity vector field measurements. *Proc. Twelfth Australasian Fluid Mechanics Conference.* 387-390.

Townsend. A.A. (1976): The structure of turbulent shear flow. *Cambridge University Press.*

Townsend. A.A. (1947): The measurement of double and triple correlation derivatives in isotropic turbulence. *Proc. Camb. Phil. Soc.* 44, 560

Vincent, A., Meneguzzi, M. (1991): The spatial structure and statistical properties of homogeneous turbulence. *J. Fluid Mech.* 225, 1-20.